# Optical Modelling of Semi-transparent OPV devices

Mushfika Baishakhi Upama, Matthew Wright, Naveen Kumar Elumalai, Md Arafat Mahmud, Dian Wang, Kah Howe Chan, Cheng Xu, Faiazul Haque, Ashraf Uddin.

School of Photovoltaic and Renewable Energy Engineering, University of New South Wales, 2052, Sydney, Australia.

***Abstract* - The optical properties of a novel semi-transparent organic solar cell were investigated to maximize photocurrent generation. The effect of multilayer anode thickness and illumination direction was studied. Optimized device can provide ~2.5 fold enhancement in photocurrent.**

***Keywords: Semi-transparent solar cell, Optical Modelling.***

## I. Introduction

Organic Photovoltaics (OPV) may become a cheap form of renewable energy, however, the lower power conversion efficiency (PCE) and shorter device lifetime means that OPV will not compete with silicon in the large power generation market in the near future. The advantages of OPV may be applicable to other applications, for example, power-generating windows [1]. This application requires a semi-transparent device structure, rather than using thick metal contacts [2], which makes the optics of the device more crucial. This report models the optics of a semi-transparent OPV device, focusing on the influence of the direction of illumination and the thickness of the electrode layer.

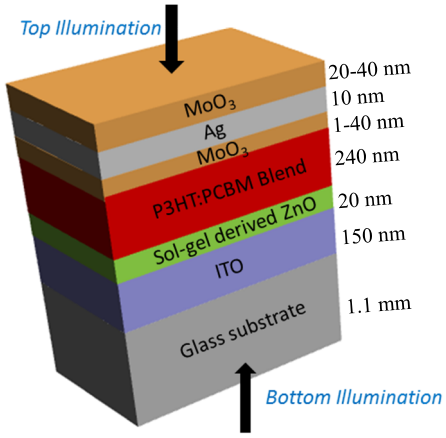


Fig. 1: Schematic diagram of device structure of the semi-transparent organic solar cell.

## II. Simulation Model and Methodology

The simulated model of the inverted semi-transparent solar cell is shown in Fig. 1. Transfer matrix modelling (TMM) was used to optimize the direction of illumination and thicknesses of the layers in the $MoO_3$/Ag/$MoO_3$ anode. A MATLAB script was developed based on the code developed by Burkhard and Hoke [3]. The optical interference of the reflected and transmitted light at each interface of the solar cell stack depends on the optical properties and thicknesses of different layers. Correspondingly, the optical constant (refractive index (n) and extinction coefficient (k)) and the thickness of each layer were given input into the TMM simulation. Based on this information, the code can enumerate the electromagnetic field distribution, the overall reflectance of the whole device and/or the multilayer anode, and the exciton generation rate in the active layer, leading to the estimation of the photocurrent.

To elucidate the effect of inner and outer $MoO_3$ layer, their thicknesses were varied systematically. One $MoO_3$ layer thickness was varied at a time while the other layer was kept constant. The reflectance of the anode and the photocurrent of the device were evaluated for each combination. The optical field distribution and the exciton generation were also computed for both bottom and top side illumination.

## III. Results and Discussion

The influence of the direction of illumination on the device optics was investigated for anode thicknesses of $MoO_3$ (6 nm)/Ag (10 nm)/ $MoO_3$ (40 nm). Fig. 2a displays the normalised electric field intensity throughout the whole device stack. For top illumination, the maximum electric field intensity occurs in the anode. The field strength reduces exponentially into the active layer region. This distribution is representative of the Beer-Lambert law of absorbance. When the device is illuminated from the bottom side, interference effects are present in the optical field distribution, which is related to the reflective multi-layer anode. A higher optical field exists in the P3HT:PCBM active layer for this case. This is confirmed by the calculated exciton generation rate, which is displayed in Fig. 2b. Table I summarizes the simulated photocurrent density ($J_{sc}$) at different $MoO_3$ layer thicknesses for both top and bottom illumination. This was calculated by assuming an internal quantum efficiency (IQE) of 100% for photons absorbed within the region form 350 – 800 nm, under AM 1.5G illumination.

In fig. 2b, an exponential reduction in exciton generation rate is observed for the top illuminated case, whilst interference phenomena are seen for bottom illumination. The exciton

978-1-4673-8603-6/16/$31.00 ©2016 IEEE

generation rate is significantly higher for cells under bottom illumination. A significant difference in simulated $J_{sc}$ reflects this observation. For optimized anode (6/10/40 nm), bottom illumination led to a simulated $J_{sc}$ value of 12.5 mA/cm$^2$, whilst top illumination only generated a $J_{sc}$ of 7.9 mA/cm$^2$.

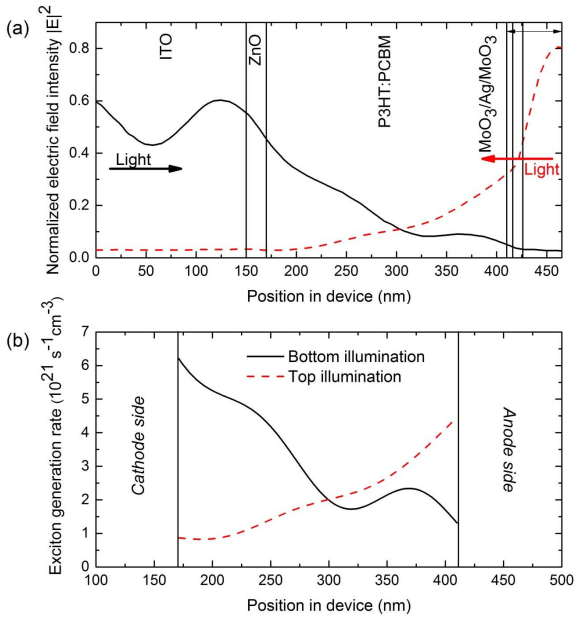


Fig. 2: (a) Spatial distribution of the normalized electric field intensity for incident light with a wavelength of 520 nm. (b) Resulting exciton generation rate profiles for AM1.5G illumination.

Next, we investigated the influence of inner and outer $MoO_3$ film thickness on the reflectance and photocurrent generation of the $MoO_3$/Ag/$MoO_3$ anode. Fig. 3a displays the reflectance for various inner $MoO_3$ thicknesses while the outer $MoO_3$ layer thickness is fixed at 40 nm. Increasing the inner film thickness from 1 – 40 nm reduces the reflectance, which reduces the $J_{sc}$ for bottom illuminated cells (Table I). The $J_{sc}$ for the 1 nm inner thickness was calculated to be 12.53 mA/cm$^2$, which reduced to 12.0 mA/cm$^2$ as the thickness increased to 40 nm. Fig. 3b displays anode reflectance for varying outer $MoO_3$ layer thickness while the inner $MoO_3$ layer thickness is fixed at 6 nm. This simulation shows that the outer layer thickness has little influence on the anode reflectance.

TABLE I
SIMULATED PHOTOCURRENT DENSITY (IN mA/cm$^2$) AT DIFFERENT $MoO_3$ LAYER THICKNESS AND ILLUMINATION DIRECTION

| Inner $MoO_3$(nm) | Bottom Illum. | Top Illum. | Outer $MoO_3$(nm) | Bottom Illum. | Top Illum. |
|---|---|---|---|---|---|
| 1 | 12.53 | 8.02 | 20 | 12.46 | 9.16 |
| 6 | 12.50 | 7.88 | 40 | 12.50 | 7.88 |
| 20 | 12.22 | 7.52 | 80 | 12.46 | 5.10 |
| 40 | 12.01 | 6.85 | - | - | - |

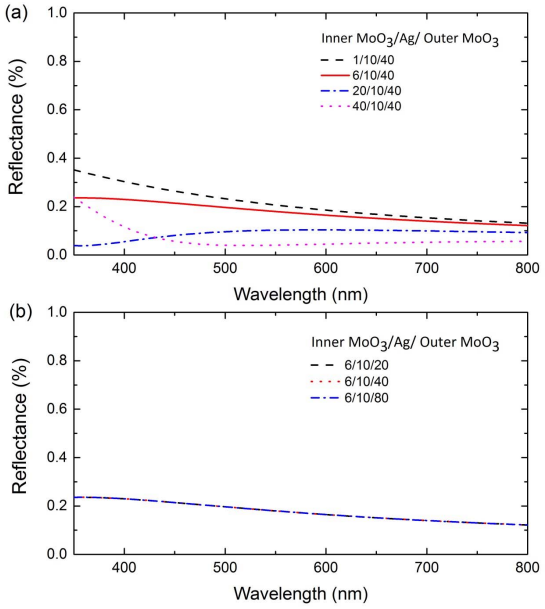


Fig. 3: Reflectance spectra of the $MoO_3$(1, 6, 20 and 40 nm)/Ag(10 nm) /$MoO_3$(20, 40, 60, 80 nm) transparent electrodes showing thickness variation of (a) inner $MoO_3$ layer and (b) outer $MoO_3$ layer.

## IV. CONCLUSION

The optical properties of a semitransparent organic solar cell were investigated using TMM. The structure contains a multi-layered anode, comprised of $MoO_3$/Ag/$MoO_3$. The simulation showed that illumination from the bottom of the device enhances the optical field in the photoactive layer, which allows for more photocurrent generation. Varying the thickness of the inner $MoO_3$ layer showed greater influence on the anode reflectance. Increasing the anode reflectance, by reducing the thickness of the inner $MoO_3$ layer, increased the photocurrent density ($J_{sc}$).

## ACKNOWLEDGMENT

The authors gratefully acknowledge the financial support of Future Solar Technologies Pty Ltd. to this project.

## REFERENCES

[1] S. Wilken, V. Wilkens, D. Scheunemann, R.-E. Nowak, K. von Maydell, J. Parisi, *et al.*, "Semitransparent Polymer-Based Solar Cells with Aluminum-Doped Zinc Oxide Electrodes," *ACS Applied Materials & Interfaces,* vol. 7, pp. 287-300, 2015/01/14 2015.

[2] J. M. Cho, S. K. Lee, S.-J. Moon, J. Jo, and W. S. Shin, "MoO3/Ag/MoO3 top anode structure for semitransparent inverted organic solar cells," *Current Applied Physics,* vol. 14, pp. 1144-1148, 8// 2014.

[3] G. F. Burkhard, E. T. Hoke, and M. D. McGehee, "Accounting for Interference, Scattering, and Electrode Absorption to Make Accurate Internal Quantum Efficiency Measurements in Organic and Other Thin Solar Cells," *Advanced Materials,* vol. 22, pp. 3293-3297, 2010.